POLYPUBLIE

Alloy disorder and partial order effects on the bowing parameter of CdZnTe semiconductors

Kan Luo, Louis Rossignol, Piotr Jakuc, Oussama Moutanabbir, Hong Guo

Document en libre accès dans PolyPublie
Open Access document in PolyPublie

Date	2026
Type	Article de revue / Article
Version	Version officielle de l'éditeur / Published version
URL de PolyPublie PolyPublie URL	https://publications.polymtl.ca/83282/
Évaluation par les pairs Peer reviewed	Révisé par les pairs / Refereed
Conditions d'utilisation Terms of use	Creative Commons Attribution 4.0 International (CC BY)
Référence Citation	Luo, K., Rossignol, L., Jakuc, P., Moutanabbir, O., & Guo, H. (2026). Alloy disorder and partial order effects on the bowing parameter of CdZnTe semiconductors. AIP Advances, 16(10), 105023 (9 pages). https://doi.org/10.1063/5.0324018

Publication officielle
Official publication

Titre de la revue Journal title	AIP Advances (vol. 16, no. 10)
Maison d'édition Publisher	American Institute of Physics
URL officielle Official URL	https://doi.org/10.1063/5.0324018
Mention légale Legal notice	© 2026 Author(s). All article content, except where otherwise noted, is licensed under a Creative Commons Attribution (CC BY) license (https://creativecommons.org/licenses/by/4.0/).

Ce fichier a été téléchargé à partir de PolyPublie, le dépôt institutionnel de Polytechnique Montréal
This file has been downloaded from PolyPublie, the institutional repository of Polytechnique Montréal
https://publications.polymtl.ca

AIP Advances

RESEARCH ARTICLE | OCTOBER 08 2026

Alloy disorder and partial order effects on the bowing parameter of CdZnTe semiconductors

Kan Luo ; Louis Rossignol ; Piotr Jakuc ; Oussama Moutanabbir ; Hong Guo

Check for updates

AIP Advances 16, 105023 (2026)
https://doi.org/10.1063/5.0324018

View Online
Export Citation

Articles You May Be Interested In

Tellurium antisites in CdZnTe

Appl. Phys. Lett. (October 2001)

$CdCl_2$ passivation of polycrystalline CdMgTe and CdZnTe absorbers for tandem photovoltaic cells

J. Appl. Phys. (May 2018)

Microphotoluminescence mapping on CdZnTe: Zn distribution

J. Appl. Phys. (July 2001)

02 November 2026 18:33:59

AIP Advances
Why Publish With Us?
19 DAYS average time to 1st decision
500+ VIEWS per article (average)
INCLUSIVE scope
Learn More
AIP Publishing

AIP Publishing

Alloy disorder and partial order effects on the bowing parameter of CdZnTe semiconductors

Cite as: AIP Advances 16, 105023 (2026); doi: 10.1063/5.0324018
Submitted: 12 March 2026 • Accepted: 23 September 2026 •
Published Online: 8 October 2026

View Online Export Citation CrossMark

Kan Luo,[1,a] Louis Rossignol,[1,b] Piotr Jakuc,[1] Oussama Moutanabbir,[2] and Hong Guo[1]

AFFILIATIONS

[1] Center for the Physics of Materials and Department of Physics, McGill University, 3600 rue University, Montreal, Quebec H3A 2T8, Canada
[2] Department of Engineering Physics, Polytechnique Montréal, 2500, chemin de Polytechnique, Montréal, Québec H3T 1J4, Canada

[a] Electronic mail: luokan1989@outlook.com
[b] Author to whom correspondence should be addressed: louis.rossignol@mail.mcgill.ca

ABSTRACT

$Cd_{1-x}Zn_xTe$ (CZT) is an important semiconductor for applications in radiation detectors. As the Zn concentration x varies, the bandgap of CZT changes accordingly, and this composition-dependent behavior is commonly described by a bowing parameter b that is independent of x. For CZT alloys, however, the measured b exhibits a broad range of values, from very small to near unity, across CZT samples fabricated by different methods, experimental conditions, and labs. Such a large variation likely originates from the microscopic details of the atomic structure in CZT. In this study, first-principles modeling is performed to theoretically investigate how atomic arrangements influence the bowing parameter. It is found that the large variation in the bowing parameter may arise from uneven atomic distributions in partially ordered configurations, which represent intermediate states between fully disordered and fully ordered alloy structures. In particular, a completely random Zn distribution is observed to yield small bowing parameters, whereas partially ordered structures tend to give rise to much larger values. By comparing ZnTe/CdTe interface models with fully disordered models, valuable insights are provided into the relationships among atomic arrangements, atomic-scale inhomogeneity, and the electronic properties of CZT. Finally, the disorder-limited resistance values of the CZT alloy models are calculated and compared.

© 2026 Author(s). All article content, except where otherwise noted, is licensed under a Creative Commons Attribution (CC BY) license (https://creativecommons.org/licenses/by/4.0/). https://doi.org/10.1063/5.0324018

02 November 2026 18:33:59

I. INTRODUCTION

The development of next-generation room-temperature detectors for high-energy radiation, such as beta rays, gamma rays, and x rays, is significant for a broad range of applications in medicine, astronomy, high-energy physics, and defense.[1–3] Over the past three decades, the Cadmium Zinc Telluride (CZT) semiconductor has emerged as the material of choice for such detectors, owing to its excellent optoelectronic properties, high atomic number, and large mass density.[4] For radiation detector applications, material homogeneity is a critical factor for achieving high performance. However, CZT materials often contain high concentrations of extended defects such as grain boundaries and Te inclusions, which can affect electronic properties and charge-carrier transport.[5] As a result, advancing crystal growth techniques to produce high-quality CZT remains a key area of research. Currently, CZT crystals can be synthesized using a variety of methods, including the Bridgman method,[6] zone refining technique,[7] vertical gradient freeze technique,[8] and traveling heater method.[9] In addition to improving crystal quality, understanding the relationship between atomic-level structure and fundamental properties is crucial for comprehending these materials and optimizing their use in detector applications.[10–12] In semiconducting pseudobinary alloys, properties such as the bandgap and lattice parameter often exhibit non-linear variation with composition. To describe this behavior, a bowing parameter b is incorporated into the equation for the bandgap of

© Author(s) 2026

CZT, $E_g(x)$, which relates it to the bandgaps of CdTe and ZnTe [E_g(CdTe) and E_g(ZnTe), respectively], and the Zn content x, as expressed in the following equation:[13]

$$E_g(x) = (1-x)E_g(\mathrm{CdTe}) + xE_g(\mathrm{ZnTe}) - bx(1-x). \quad (1)$$

Equation (1) is very useful for optoelectronic applications, as it gives the bandgap of the CZT crystal for any Zn concentration x. Numerous experimental studies have been conducted to determine the bowing parameter b of CZT. Hsu *et al.* grew $Cd_{1-x}Zn_xTe$ mixed crystals with the Zn content x ranging from 0 to 1 using a high-temperature and high-pressure vertical Bridgman–Stockbarger method, reporting a measured bowing parameter of 0.376 eV.[14] Reno and Jones reported an experimental bowing parameter of 0.460 eV based on photoluminescence spectra of epitaxial $Cd_{1-x}Zn_xTe$ thin films.[15] Kartopu *et al.* synthesized polycrystalline $Cd_{1-x}Zn_xTe$ thin films using metalorganic chemical vapor deposition (MOCVD) and reported bowing parameters around 0.7 and 0.3 eV from optical and photoluminescence spectra.[16] Using the Tran–Blaha modified Becke–Johnson (mBJ) potential to determine electronic properties, Mimouni *et al.* obtained a bandgap bowing parameter of $b \approx 0.46$ eV for the $Cd_{1-x}Zn_xTe$ alloy and found that volume deformation is the main reason for the bowing effect.[17] In fact, these and other previous investigations reported CZT to have a range of bowing parameters, ranging from 0 to 0.9 eV across different samples.[18–21] This is unlike other binary semiconductors for which a relatively constant bowing parameter can be experimentally determined.[22] Some theoretical studies have attempted to elucidate this puzzling behavior by employing the virtual crystal approximation (VCA) models or special quasi-random structures[23] (SQS) to calculate the bowing parameter.[24,25] Nevertheless, the underlying causes of these inconsistencies remain unclear and warrant further analysis, as the VCA model overlooks atomic distribution and SQS only accounts for the bowing parameter in fully disordered configurations.

In this study, we propose and theoretically verify by first-principles modeling that the broad variation in the bowing parameter for CZT likely arises from the uneven microscopic atomic arrangements of Cd and Zn. While fully disordered and fully ordered configurations exhibit uniform atomic distribution patterns, the actual structural scenario of CZT may lie between these extreme states, represented by partially ordered configurations. Modeling such partially ordered (PO) configurations turns out to present some significant challenges. Indeed, it is known that the bandgap is strongly dependent on stress-induced lattice deformation, and varying the Zn content leads to significant changes in the lattice parameter. Therefore, it is possible that experimental CZT materials contain clustered regions of CdTe and ZnTe that induce lattice deformation, causing variations in the bowing parameter. To model the clustering effect, we use partially ordered (PO) structures. Ideally, PO structures are CZT crystals containing nonuniform regions of CdTe and ZnTe. Such PO structures require substantial computational resources for density functional theory (DFT) calculations. Therefore, to reduce the prohibitive computational cost and obtain a qualitative picture, we mimic the non-uniformity using simple interface models (Fig. 2), using layers to represent clustering of different concentrations for given supercell sizes. Note that there are essentially infinite possibilities to choose from, and we pick the simplest structure to study the idea that the wide range of the observed bowing parameters may be related to clustering effects. Our results indicate that partially ordered configurations increase the bowing parameter from 0.3 to 0.7 eV, which suggests that the broad range of the bowing parameters observed experimentally may be related to these partially ordered CZT structures. In addition, isotropic pressure reduces the bowing parameter in disordered configurations while increasing it in partially ordered configurations, which is attributed to the different bulk moduli of ZnTe and CdTe. Through band-structure and resistance calculations, this study reveals that partially ordered configurations can trap carriers, leading to reduced detector performance. Our atomistic modeling provides valuable insights into the complex interplay between atomic-scale structure and electronic properties, offering practical suggestions for designing CZT-based devices with optimized properties for applications in radiation detection and beyond.

II. SYSTEM AND CALCULATION METHODS

In this study, completely disordered CZT configurations are modeled using a $3 \times 3 \times 3$ supercell containing 216 atoms, generated via the SQS method to randomize Zn/Cd occupations. The SQS method, designed for modeling disordered occupancy systems, identifies a special, nearly random configuration within a supercell of a specified size, which has been effective in numerous calculations of disordered alloy structures.[26,27] This modeling process is implemented using the *mcsqs* package within the Alloy Theoretic Automated Toolkit (ATAT),[28] which is employed to identify the optimal disordered configurations. The CZT configurations with Zn content x values of 0 (a), 1/6 (b), 1/4 (c), 10/27 (d), 1/2 (e), 17/27 (f), 3/4 (g), and 5/6 (h) are illustrated in Fig. 1. To model the statistically random alloy, the pair correlations within 14 Å, triplet correlations within 8 Å, and quadruplet correlations within 6 Å in the SQS supercells are adopted. The optimization procedure was terminated when the objective function reached a threshold value below −2.99. It is useful to mention that more negative values mean better quality at the cost of increased computational time, so a moderately chosen value is picked to generate an adequate SQS configuration. In addition, the configuration with $x = 1$ is derived from the $x = 0$ configuration by replacing Cd with Zn. It is evident that Zn and Cd atoms are randomly distributed within the supercells, with no distinct ZnTe/CdTe clusters or interfaces observed. The disordered configurations in Fig. 1 are called SQS-configurations in the rest of this paper.

In contrast to the SQS configurations, the PO configurations exhibit an uneven distribution of Zn and Cd atoms in the supercell, leading to local concentration differences of Zn and Cd. Due to a positive mixing energy between ZnTe and CdTe, these concentration inhomogeneities may tend to form clusters with varying Zn/Cd contents. The first-principles analysis of such cluster models is extremely challenging, as it requires a huge number of atoms within the supercell, making property calculations prohibitively expensive. In this study, we shall focus on the inevitable interfaces between concentration differences across atomic clusters by creating ZnTe/CdTe interfaces along specific crystallographic planes. Crystals tend to cleave along low-index and low-energy planes. In

02 November 2026 18:33:59

© Author(s) 2026

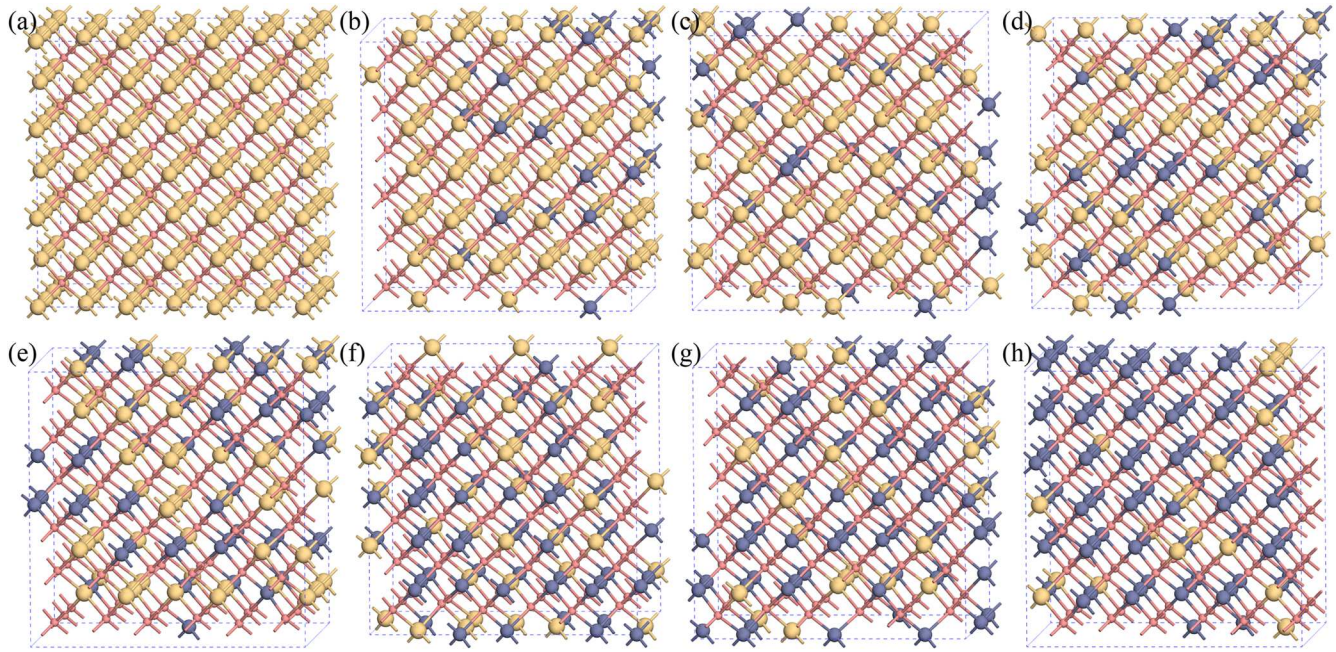


FIG. 1. Disordered CdZnTe configurations with the Zn content x values of 0 (a), 1/6 (b), 1/4 (c), 10/27 (d), 1/2 (e), 17/27 (f), 3/4 (g), and 5/6 (h) generated via the SQS method, where bisque, royal blue, and pink spheres represent Cd, Zn, and Te atoms, respectively.

02 November 2026 18:33:59

cubic structures, these planes include [100], [110], and [111] orientations. For instance, CdTe frequently develops dislocations on its (111), (110), and (001) surfaces.[29] We therefore investigate the limiting cases of the simplest possible PO-configurations as shown in Fig. 2, where interfaces are oriented along the [100] direction, and the ZnTe regions increase incrementally layer by layer, corresponding to Zn content fractions of 1/6, 1/3, 1/2, 2/3, and 5/6. Similarly, the ZnTe/CdTe interface models along the [110] and [111] directions are shown in Figs. S1 and S2, respectively. In the rest of this paper, these are called ZnTe/CdTe PO-configurations. These configurations are supercells periodically extended to form crystals, and doubling the size of the supercell while keeping the Zn content the same does not change the calculated bowing parameter. The purpose is to use this simple model to mimic the nonuniform distribution of ZnTe and CdTe clustering and qualitatively examine the effects of such non-uniformity on the bowing parameter. Effects of more realistic clustering on the bowing parameter in GaAs alloyed with Sb were studied using an empirical tight-binding model.[30] Such clustering could be a path toward future developments.

To assess the energy changes in the SQS-configurations and ZnTe/CdTe PO-configurations, a mixing energy ΔE is defined by the following equation, where E_{CZT} represents the calculated total energy of the CZT alloy, and E_{CdTe} and E_{ZnTe} correspond to the energies of CdTe and ZnTe in the same crystal structure:

$$\Delta E = E_{CZT} - [(1-x)E_{CdTe} + xE_{ZnTe}]. \quad (2)$$

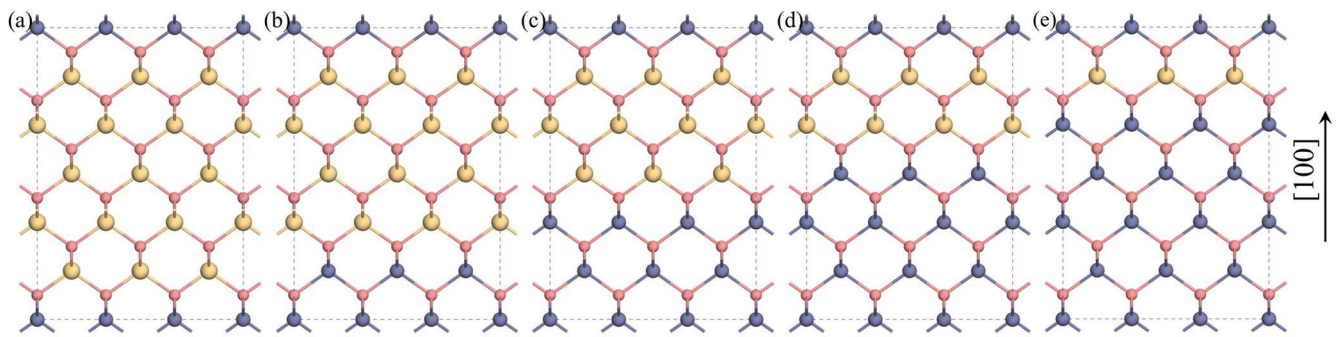


FIG. 2. Partially ordered structures along the [100] direction with the Zn content x of 1/6 (a), 1/3 (b), 1/2 (c), 2/3 (d), and 5/6 (e), respectively.

© Author(s) 2026

The atomic positions and cell parameters are optimized using the Vienna *Ab initio* Simulation Package (VASP),[31] employing projector-augmented-wave (PAW)[32] potentials. A generalized gradient approximation (GGA)[33] for the exchange-correlation energy with the Perdew–Burke–Ernzerhof (PBE) functional[34] is employed, and a plane-wave energy cutoff of 550 eV is applied to describe the electronic wave functions in these calculations. To obtain more reliable electronic structure predictions, after the structural relaxation, electronic band structures are obtained by a real-space Kohn–Sham DFT solver, RESCU (Real space Electronic Structure CalcUlator),[35] employing DZP basis pseudopotentials and the more accurate exact exchange HSE06 hybrid functional,[36,37] which corrects the underestimated bandgap of the semilocal PBE functional. We note in passing that another relatively simple approach to correct the underestimated bandgap is to use the GGA + U method. The calculated band structures of CdTe and ZnTe in their primitive cells are presented in Fig. S3. The computed bandgaps of 1.46 eV for CdTe and 2.14 eV for ZnTe are consistent with previously reported values.[24]

The ballistic resistance values of the CZT alloys are calculated using a two-terminal device structure in which the central device region is the CZT alloy material. This is performed by the nonequilibrium Green's function (NEGF) formalism as implemented in the NanoDCAL quantum transport package.[38] In the NEGF formalism, the density matrix is computed by Eq. (3), where the lesser Green's function $G^<$ satisfies the Keldysh equation $G^< = G^R\Sigma^<G^A$, the retarded Green's function $G^R = (G^A)^\dagger$ is related to the system's Hamiltonian, and the lesser self-energy $\Sigma^<$ represents the injection of charge from the electrodes to the central region in the two-terminal transport junction,

$$\rho = -\frac{i}{2\pi}\int G^<(E)dE. \tag{3}$$

After the NEGF-DFT self-consistency is achieved, the transmission coefficient $T(E)$ is calculated according to Eq. (4), where E is the electron energy and Γ_l and Γ_r represent the coupling of the central region of the two-terminal junction to the left and right electrodes, respectively,

$$T(E) = T_r(\Gamma_l G^R \Gamma_r G^A). \tag{4}$$

Then the conductance G is obtained at the Fermi level E_F by Eq. (5), where e is the elementary charge and h is Planck's constant,

$$G = \frac{2e^2}{h}T(E_F). \tag{5}$$

The resistance R is obtained as $R = 1/G$.

III. RESULTS AND DISCUSSION

The optimized lattice constants of disordered CZT in SQS-configurations depicted in Fig. 1, under various pressures, are presented in Fig. 3(a). The results reveal that the effect of pressure on CZT is largely consistent across different compositions x. The calculated lattice constants for CdTe and ZnTe are 6.624 and 6.183 Å at 0 GPa, respectively, which agree well with previously reported theoretical and experimental values.[39,40]

The lattice mismatch between CdTe and ZnTe is ~5.8%, which places this system in the moderate-mismatch regime (1%–7%). For cubic crystal structures, the interplanar spacing is given by $d = a/\sqrt{h^2 + k^2 + l^2}$, where a is the lattice parameter and (hkl) are the Miller indices. While the presence of two atomic species (Cd/Zn and Te) in CdZnTe means that the surface energetics are influenced by factors beyond the interplanar spacing, the general trend remains that lower-index planes exhibit lower surface/interface energies. Our mixing energy calculations reveal that the [111] orientation exhibits significantly higher mixing energy as compared to both the [100] and [110] directions. Due to the cubic symmetry of the system, the [100], [010], and [001] directions are crystallographically equivalent, as are their related families of planes. Therefore, we focused on the three fundamental low-index orientations [100], [110], and [111],

02 November 2026 18:33:59

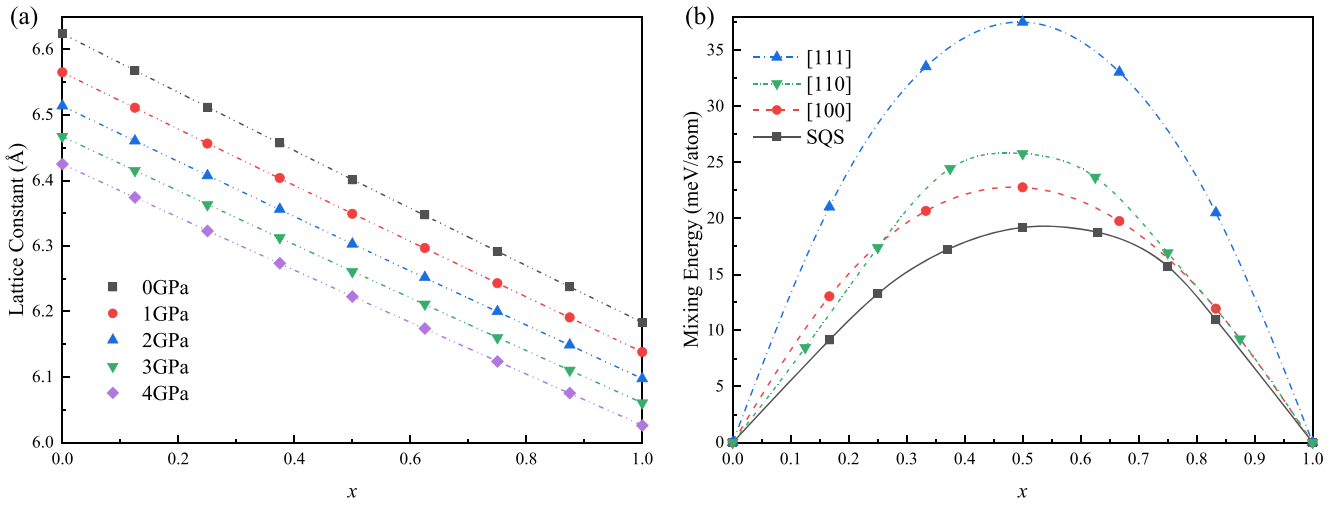


FIG. 3. (a) The variation of the lattice constant in CZT as a function of Zn content x under different pressures. (b) The mixing energy of disordered and partially ordered CZT, including the interface models along the [100], [110], and [111] directions, as a function of Zn content x.

© Author(s) 2026

which provide a reasonable representation of the anisotropic properties in this material system. Under a given pressure, the lattice constants of the SQS-configurations exhibit a nearly perfect linear relationship with Zn content x, indicating that the bowing parameter of the bandgap does not arise from lattice constant variations. The mixing energy of the SQS- and PO-configurations of CZT is shown in Fig. 3(b). The positive values of mixing energy indicate that CZT is thermodynamically prone to decomposition into CdTe and ZnTe, which explains the material's tendency to exhibit compositional inhomogeneity. Through systematic DFT analysis of the mixing energetics of CZT, we found that the SQS-configurations consistently exhibit better thermodynamic stability compared to both the PO and the random configurations across the entire Zn composition range, suggesting that SQS configurations provide a physically representative model for completely disordered CdZnTe alloys.

The SQS-configurations of CZT exhibit lower mixing energy compared to the PO-configurations. The energy difference is relatively small, amounting to a few meV/atom higher for PO-configurations with interfaces along the [100] and [110] directions. In contrast, PO-configurations with interfaces along the [111] direction show the highest mixing energy, suggesting that concentration gradient-driven interfaces are more likely to form along the [100] and [110] directions. This difference may arise from the larger lattice mismatch of the (111) surface, which features smaller interlayer atomic distances and a larger primitive basis compared to the (100) and (110) surfaces. Our calculations of the mixing energy across the 1–4 GPa pressure range (Fig. S4) demonstrate that the formation enthalpy of the alloy remains virtually constant. This pressure independence clearly indicates that applied pressure has minimal influence on both the thermodynamic stability and fundamental

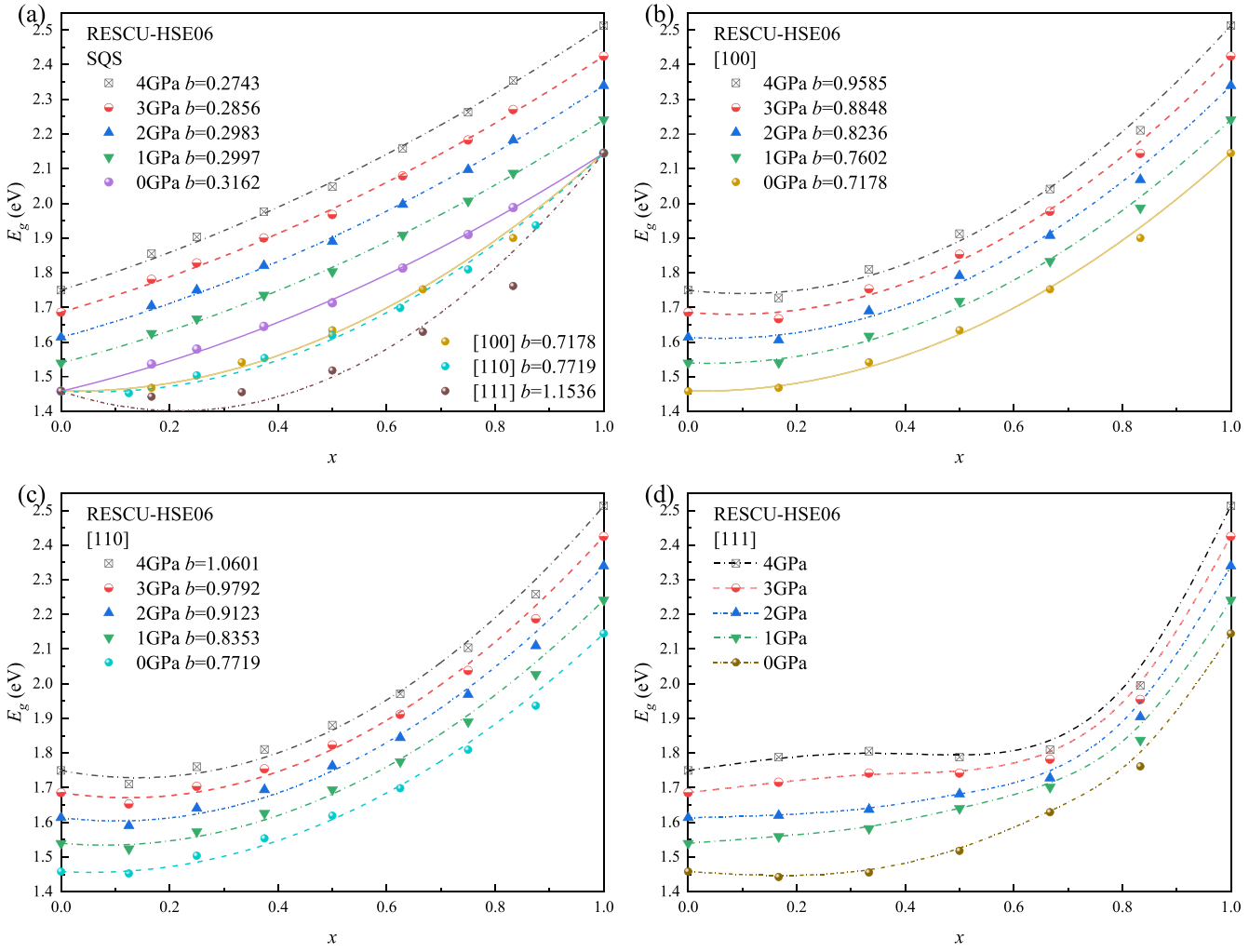


FIG. 4. Bandgap variation of CZT as a function of Zn content x at different pressures: (a) SQS-configurations, (b) PO-configurations along [100], (c) PO-configurations along [110], and (d) PO-configurations along [111].

02 November 2026 18:33:59

© Author(s) 2026

properties of CZT. These computational results suggest that achieving high-quality CZT requires identifying methods at the atomic scale to minimize the mixing energy or to enhance the energy difference between PO-configurations and SQS-configurations. This objective could potentially be realized through strategic doping of additional elements.[41]

The variation in Zn and Cd arrangements significantly influences the electronic structure of CZT. The HSE06 bandgap results for SQS-configurations of CZT are presented in Fig. 4(a), where the bowing parameter is determined to be 0.3162 eV at 0 GPa and decreases with increasing pressure, reaching 0.2743 eV at 4 GPa, indicating that the bowing parameter of SQS-configurations of CZT remains close to 0.3 eV across the pressure range. For these configurations, the effects of pressure on Cd–Te and Zn–Te bond lengths are nearly identical, with both being compressed by similar ratios under a given pressure. Consequently, the bowing parameter exhibits minimal variation across different pressures. In contrast, the PO-configurations of CZT containing ZnTe/CdTe interfaces along the [100], [110], and [111] directions exhibit significantly higher bowing parameters at 0 GPa: 0.7178, 0.7719, and 1.1536 eV, respectively. The bowing parameters increase notably under pressure, as shown in Figs. 4(b)–4(d), suggesting that the partially ordered configurations can exhibit a bowing parameter around 0.7 eV. Notably, for the PO-configuration along the [111] direction, the curve deviates from a quadratic trend under pressure. These results further reveal that disordered and partially ordered CZT exhibit entirely opposite trends in the bowing parameter under pressure. This variation can be attributed to differences in the bulk moduli of CdTe and ZnTe. The CdTe regions, with their larger lattice constants and lower elastic constants,[42,43] are more susceptible to pressure. The compression of these regions leads to lattice constants approaching those of ZnTe, narrowing the bandgap and thereby increasing the bowing parameter.

The larger bowing parameter in PO-configurations of CZT can be attributed to differing contributions of Cd to the valence bands, as shown in the calculated density of states (DOS) in Fig. S5. For the same Zn and Cd composition in $Cd_{0.5}Zn_{0.5}Te$, the contributions of Cd and Zn to the valence and conduction bands differ significantly between SQS- and PO-configurations. In the SQS configuration, the contributions of Cd and Zn to the valence and conduction bands are nearly identical. However, in the PO-configurations, Cd exhibits a significantly higher contribution, particularly in the valence bands. Due to the smaller bandgap of CdTe, the overall bandgap of the bulk CZT is therefore reduced compared to that of the SQS configuration, resulting in a larger bowing parameter.

Using the NEGF-DFT transport package and Eq. (5), we also calculated the ballistic resistance R of CdTe, ZnTe, ZnTe/CdTe PO-configurations, and disordered SQS-configurations of $Cd_{0.5}Zn_{0.5}Te$, with and without VCA doping. The calculated resistance values are summarized in Table I. The undoped resistance ranges from 0.1×10^{16} to 74×10^{16} Ω in different directions. Typically, a semiconductor exhibits very high undoped resistance, which sharply decreases when doped with holes or electrons. The calculated resistances of CdTe and ZnTe corroborate this behavior, and introducing a dopant concentration of 10^{-5} (holes or electrons) reduces the resistance by nearly ten orders of magnitude. However, the situation is different for holes in the ZnTe/CdTe PO-configurations. The resistance values are about five orders of magnitude higher than those in CdTe and ZnTe with the same hole doping concentration, indicating a barrier for hole carriers; meanwhile, no significant trapping effects are observed for electrons. This barrier may arise from the slightly lower energy of hole carriers in CdTe than in ZnTe. As shown in Fig. 5, the valence bands of ZnTe and CdTe exhibit an offset, creating a step-like energy barrier for holes. Consequently, the carriers tend to flow into and become trapped in the CdTe region, which leads to higher resistance.

02 November 2026 18:33:59

TABLE I. Calculated ballistic resistance values for two-probe transport junctions of CdTe, ZnTe, the CdTe/ZnTe interface, and $Cd_{0.5}Zn_{0.5}Te$ in the undoped case and with VCA doping at a concentration of 10^{-5}. L and S denote the junction length and cross-sectional area, respectively.

R (Ω)	Index	p-type ($\times 10^6$)	n-type ($\times 10^6$)	Undoped ($\times 10^{16}$)	S (Å^2)	L (Å)
CdTe	[100]	0.7673	0.6638	0.1207	87.76	19.87
	[110]	2.2265	0.4726	0.1085	124.12	18.74
	[111]	3.7165	0.7701	0.3997	76.01	22.95
ZnTe	[100]	0.7783	0.6946	1.0813	76.46	18.55
	[110]	0.7780	0.4903	0.9567	108.14	17.49
	[111]	1.3459	0.8431	5.1795	66.22	21.42
ZnTe/CdTe interface	[100]	5.11×10^5	2.1002	0.1662	81.42	19.42
	[110]	3.64×10^4	0.6454	0.2023	115.23	18.20
	[111]	5.71×10^4	1.0224	0.6653	70.78	22.35
$Cd_{0.5}Zn_{0.5}Te$	[100]	2.6966	0.7539	0.9570	81.96	19.10
	[110]	72.818	0.5060	0.1960	115.91	18.00
	[111]	3.3957	0.8636	1.3266	70.98	22.07
	Σ3 [111]	3.1775	0.8226	5.9878	141.96	44.31
	Σ5 [012]	13.300	6.0148	73.995	91.63	57.27

© Author(s) 2026

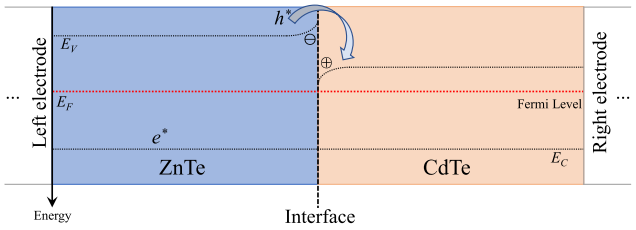


FIG. 5. Schematic diagram of the positions of ZnTe and CdTe relative to the Fermi level for hole carriers.

This trapping effect can be further demonstrated through various doping strategies. With the same ZnTe/CdTe [100] interface model, increasing the doping concentration from 10^{-5} to 10^{-4} leads to a slight reduction in resistance to 8.87×10^{10} Ω, while a doping concentration of 10^{3} further reduces the resistance to 2.68×10^{6} Ω, as the carrier concentration becomes sufficient to overcome the energy barrier in the CdTe region. If holes with a concentration of 10^{-5} are exclusively doped at the ZnTe site, the resistance reaches 8.49×10^{11} Ω, comparable to the *p*-type doping value shown in Table I. In contrast, doping the CdTe site results in a resistance of 1.72×10^{15} Ω, similar to the undoped configuration, thereby confirming the presence of a trapping effect in the CdTe region. We conclude that microstructural inhomogeneity significantly impedes carrier transport in CZT and degrades performance in detector applications.

Finally, grain boundaries may also exist in the PO-configurations. Using the Coincidence Site Lattice (CSL) grain boundary (GB) models along the [111] and [012] directions, we carried out a preliminary calculation of the resistance of Σ3 and Σ5 twin GBs. The results indicate that the resistance of undoped GB structures is higher than that of the bulk crystal and PO-configurations of the alloy. However, for hole- and electron-doped structures (via VCA), the resistance shows minimal differences compared to the bulk and PO-configurations. This suggests that the impact of GBs on resistance primarily arises from structural changes in the lattice and increased atomic contact distances, rather than directly affecting carrier mobility. The accumulation of carriers at GBs is likely influenced by compositional inhomogeneities formed near the interfaces. In addition, the CSL models, which consist of only a few hundred atoms, may not fully capture the GB structures. We hope to address this limitation in a future study.

IV. CONCLUSIONS

In summary, this study investigates the electronic properties of CZT alloys, with a focus on the effects of pressure, band structure, and doping on completely disordered SQS configurations and partially ordered interface configurations. HSE06 bandgap calculations reveal contrasting trends in the bowing parameter of CZT under pressure for these configurations. SQS-configurations of CZT exhibit a lower bowing parameter (0.3162 at 0 GPa) that decreases with pressure, while PO-configurations of CZT with [100], [110], and [111] interfaces show significantly higher bowing parameters (0.7178, 0.7719, and 1.1536 eV, respectively) that increase under pressure. This contrasting behavior is attributed to variations in Cd content in the valence bands, arising from the smaller bandgap of CdTe as compared to that of ZnTe. These findings suggest that the experimentally observed variation in the bowing parameter reflects the degree of disorder and partial order within the CZT alloy material, offering a possible explanation for the broad range of bowing parameters of CZT across different experiments. The quality of the CZT alloy can be improved by doping additional elements, which reduce the system's mixing energy and increase the energy difference between partially ordered and disordered structures.

Ballistic resistance calculations show that undoped CZT has very high resistance, ranging from 0.1×10^{16} to 74×10^{16} Ω, which decreases significantly with hole or electron doping. Surprisingly, partially ordered CZT with ZnTe/CdTe interfaces has higher resistance for hole carriers than completely disordered CZT. This behavior is attributed to a carrier trapping effect, where holes are confined within the CdTe region due to its lower hole energy relative to ZnTe. This trapping effect is further validated through doping concentration studies, which highlight the influence of doping levels on resistance. These findings emphasize the critical role of atomic arrangement, microstructural inhomogeneity, and doping in shaping the transport properties of the CZT alloy. The insights gained from this study offer valuable guidance for designing CZT-based materials with optimized electronic properties, particularly for applications in radiation detection and beyond.

SUPPLEMENTARY MATERIAL

See the supplementary material for the partially ordered configurations along the [110] and [111] directions and the band structures of CdTe and ZnTe in primitive cells using RESCU within the HSE06 functional.

ACKNOWLEDGMENTS

We acknowledge Jyun-Jie Jiang, ShuaiShuai Yuan, and Songqi Jia for the discussions about the CZT modeling (K.L. and H.G.). This research was funded by an Alliance Grant of the Natural Sciences and Engineering Research Council (NSERC) of Canada (H.G. and O.M.) and the Fonds de recherche du Québec-Nature et technologies (FRQNT) of the Province of Quebec (H.G.). We acknowledge the Digital Research Alliance of Canada and the High-Performance Computing Center of McGill University for the computing facilities that made this study possible.

AUTHOR DECLARATIONS

Conflict of Interest

The authors have no conflicts to disclose.

Author Contributions

K.L., **H.G.**, and **O.M.**: conceptualization of the investigation, the method of investigation, the data analysis, and the paper draft.

02 November 2026 18:33:59

© Author(s) 2026

K.L. led the DFT calculations and data collection. **L.R.** and **P.J.** participated in the atomic model construction, DFT calculations, data collection, and editing of the paper.

Kan Luo: Conceptualization (equal); Data curation (equal); Formal analysis (equal); Investigation (equal); Methodology (equal); Supervision (equal); Validation (equal); Visualization (equal); Writing – original draft (equal); Writing – review & editing (equal). **Louis Rossignol**: Formal analysis (equal); Investigation (equal); Methodology (equal); Software (equal); Writing – original draft (equal); Writing – review & editing (equal). **Piotr Jakuc**: Formal analysis (equal); Investigation (equal); Methodology (equal); Software (equal); Writing – original draft (equal); Writing – review & editing (equal). **Oussama Moutanabbir**: Formal analysis (equal); Investigation (equal); Supervision (equal); Validation (equal); Writing – original draft (equal); Writing – review & editing (equal). **Hong Guo**: Conceptualization (equal); Formal analysis (equal); Funding acquisition (equal); Investigation (equal); Methodology (equal); Project administration (equal); Supervision (equal); Validation (equal); Writing – original draft (equal); Writing – review & editing (equal).

DATA AVAILABILITY

The data supporting the findings of this study are available within the article and its supplementary material. In addition, a more detailed table is available online, providing information on the crystals and the data-processing procedure used to convert the NEGF-DFT software output into the results presented in Table I.

REFERENCES

[1] S. Miyajima, K. Imagawa, and M. Matsumoto, "CdZnTe detector in diagnostic x-ray spectroscopy," Med. Phys. **29**(7), 1421–1429 (2002).
[2] B. Park, J. Ko, J. Byun, B. Park, M.-J. Lee, and J. Kim, "Feasibility study of CdZnTe and CdZnTeSe based high energy X-ray detector using linear accelerator," Nucl. Eng. Technol. **55**(8), 2797–2801 (2023).
[3] X. Wan, Y. Kang, H. Wei, R. Jiang, Y. Liu, R. Cheng, X. Tian, T. Tan, G. Zha, Y. Li, and K. Cao, "Improvement of radiation detection performance of a detector prepared by CdZnTe epitaxial single crystal," Radiat. Meas. **175**, 107177 (2024).
[4] U. N. Roy, A. Gueorguiev, S. Weiller, and J. Stein, "Growth of spectroscopic grade $Cd_{0.9}Zn_{0.1}Te$:In by THM technique," J. Cryst. Growth **312**(1), 33–36 (2009).
[5] A. E. Bolotnikov, G. S. Camarda, Y. Cui, G. Yang, A. Hossain, K. Kim, and R. B. James, "Characterization and evaluation of extended defects in CZT crystals for gamma-ray detectors," J. Cryst. Growth **379**, 46–56 (2013).
[6] L. Abbene, F. Principato, G. Gerardi, A. Buttacavoli, D. Cascio, M. Bettelli, N. S. Amadè, P. Seller, M. C. Veale, O. Fox, K. Sawhney, S. Zanettini, E. Tomarchio, and A. Zappettini, "Room-temperature X-ray response of cadmium-zinc-telluride pixel detectors grown by the vertical Bridgman technique," J. Synchrotron Radiat. **27**(2), 319–328 (2020).
[7] H. H. Woodbury and R. S. Lewandowski, "Improved sealed-ingot zone refining technique for growth of CdTe crystals," J. Cryst. Growth **10**(1), 6–12 (1971).
[8] H. Bensalah, J. Crocco, V. Carcelén, A. Black, Q. Zheng, J. L. Plaza, and E. Diéguez, "Effect of superheating and fast cooling on Te inclusions of $Cd_{0.9}Zn_{0.1}Te$:In crystals grown by vertical gradient freezing," J. Cryst. Growth **361**, 5–10 (2012).
[9] L. Abbene, G. Gerardi, G. Raso, F. Principato, N. Zambelli, G. Benassi, M. Bettelli, and A. Zappettini, "Development of new CdZnTe detectors for room-temperature high-flux radiation measurements," J. Synchrotron Radiat. **24**(2), 429–438 (2017).
[10] D. Åberg, P. Erhart, and V. Lordi, "Contributions of point defects, chemical disorder, and thermal vibrations to electronic properties of $Cd_{1-x}Zn_xTe$ alloys," Phys. Rev. B **88**, 045201 (2013).
[11] H. Duan, X. Chen, Y. Huang, X. Zhou, L. Sun, and W. Lu, "Composition-dependent electronic properties, optical transitions, and anionic relaxations of $Cd_{1-x}Zn_xTe$ alloys from first principles," Phys. Rev. B **76**, 035209 (2007).
[12] H. Duan, X. S. Chen, Y. Huang, L. Wang, and W. Lu, "First-principles study of fundamental properties and electronic structure of $Cd_{1-x}Zn_xTe$ alloys," Phys. Lett. A **370**(5–6), 517–521 (2007).
[13] J. Yang and W. Su-Huai, "First-principles study of the band gap tuning and doping control in $CdSe_xTe_{1-x}$ alloy for high efficiency solar cell," Chin. Phys. B **28**(8), 086106 (2019).
[14] H. P. Hsu, D. Y. Lin, C. W. Chen, Y. F. Wu, K. Strzałkowski, and P. Sitarek, "Optical characterizations of $Cd_{1-X}Zn_XTe$ mixed crystals grown by vertical Bridgman-Stockbarger method," J. Cryst. Growth **534**, 125491 (2020).
[15] J. L. Reno and E. D. Jones, "Determination of the dependence of the band-gap energy on composition for $Cd_{1-x}Zn_xTe$," Phys. Rev. B **45**, 1440–1442 (1992).
[16] G. Kartopu, Q. Fan, O. Oklobia, and S. J. C. Irvine, "Combinatorial study of the structural, optical, and electrical properties of low temperature deposited $Cd_{1-x}Zn_xTe$ ($0 \leqslant x \leqslant 1$) thin films by MOCVD," Appl. Surf. Sci. **540**, 148452 (2021).
[17] K. Mimouni, N. Mokdad, K. Beladjal, A. Kadri, and K. Zitouni, "Energy bandgap of $Cd_{1-x}Zn_xTe$, $Cd_{1-x}Zn_xSe$ and $Cd_{1-x}Zn_xS$ semiconductors: A first-principles analysis based on Tran–Blaha–modified Becke–Johnson exchange potential," J. Electron. Mater. **52**(6), 4191–4201 (2023).
[18] O. Zelaya-Angel, J. G. Mendoza-Alvarez, M. Becerril, H. Navarro-Contreras, and L. Tirado-Mejía, "On the bowing parameter in $Cd_{1-x}Zn_xTe$," J. Appl. Phys. **95**(11), 6284–6288 (2004).
[19] A. H. Ammar, "Structural and optical properties of $Zn_xCd_{1-x}Te$ thin films," Physica B **296**(4), 312–318 (2001).
[20] L. Tirado-Mejía, J. I. Marín-Hurtado, and H. Ariza-Calderón, "Influence of disorder effects on $Cd_{1-x}Zn_xTe$ properties," Phys. Status Solidi B **220**(1), 255–260 (2000).
[21] H. C. Poon, Z. C. Feng, Y. P. Feng, and M. F. Li, "Relativistic band structure of ternary II-VI semiconductor alloys containing Cd, Zn, Se, and Te," J. Phys.: Condens. Matter **7**(14), 2783 (1995).
[22] T. Sandu and R. I. Iftimie, "Bandgaps and band bowing in semiconductor alloys," Solid State Commun. **150**(17-18), 888–892 (2010).
[23] A. Zunger, S.-H. Wei, L. G. Ferreira, and J. E. Bernard, "Special quasirandom structures," Phys. Rev. Lett. **65**, 353 (1990).
[24] I. Khan, H. A. R. Aliabad, W. Ahmad, Z. Ali, and I. Ahmad, "First principle optoelectronic studies of visible light sensitive CZT," Superlattices Microstruct. **63**, 91–99 (2013).
[25] D. W. Niles and H. Höchst, "Determination of the bowing parameter of the split-off band in $Cd_{0.8}Zn_{0.2}Te(100)$ by angle-resolved photoemission spectroscopy," Phys. Rev. B **46**, 1498–1504 (1992).
[26] S. H. Wei, L. G. Ferreira, J. E. Bernard, and A. Zunger, "Electronic properties of random alloys: Special quasirandom structures," Phys. Rev. B **42**, 9622–9649 (1990).
[27] K. A. Mäder and A. Zunger, "Short- and long-range-order effects on the electronic properties of III-V semiconductor alloys," Phys. Rev. B **51**, 10462–10476 (1995).
[28] A. van de Walle, "Multicomponent multisublattice alloys, nonconfigurational entropy and other additions to the alloy theoretic automated toolkit," Calphad **33**(2), 266–278 (2009).
[29] H. S. Leipner, J. Schreiber, H. Uniewski, and S. Hildebrandt, "Dislocation luminescence in cadmium telluride," Scanning Microsc. **12**(1), 149–160 (1998).
[30] A.-L. Phan, A. Pecchia, A. Di Vito, and M. Auf der Maur, "Empirical tight-binding method for large-supercell simulations of disordered semiconductor alloys," Phys. Scr. **99**, 075903 (2024).
[31] J. Hafner, "*Ab-initio* simulations of materials using VASP: Density-functional theory and beyond," J. Comput. Chem. **29**(13), 2044–2078 (2008).
[32] G. Kresse and D. Joubert, "From ultrasoft pseudopotentials to the projector augmented-wave method," Phys. Rev. B **59**, 1758–1775 (1999).
[33] J. P. Perdew, J. A. Chevary, S. H. Vosko, K. A. Jackson, M. R. Pederson, D. J. Singh, and C. Fiolhais, "Atoms, molecules, solids, and surfaces: Applications of

02 November 2026 18:33:59

© Author(s) 2026

the generalized gradient approximation for exchange and correlation," Phys. Rev. B **46**, 6671–6687 (1992).
[34]J. P. Perdew, K. Burke, and M. Ernzerhof, "Generalized gradient approximation made simple," Phys. Rev. Lett. **77**(18), 3865–3868 (1996).
[35]V. Michaud-Rioux, L. Zhang, and H. Guo, "RESCU: A real-space electronic structure method," J. Comput. Phys. **307**, 593–613 (2016).
[36]J. Heyd, G. E. Scuseria, and M. Ernzerhof, "Hybrid functionals based on a screened Coulomb potential," J. Chem. Phys. **118**(18), 8207–8215 (2003).
[37]J. Paier, M. Marsman, K. Hummer, G. Kresse, I. C. Gerber, and J. G. Ángyán, "Screened hybrid density functionals applied to solids," J. Chem. Phys. **124**(15), 154709 (2006).
[38]J. Taylor, H. Guo, and J. Wang, "*Ab initio* modeling of quantum transport properties of molecular electronic devices," Phys. Rev. B **63**, 245407 (2001).
[39]D. Liu, J. Feng, M. Tian, Q. Li, and R. Sa, "First-principles study of the stability, electronic and optical properties of CdTe under hydrostatic pressure," Chem. Phys. Lett. **764**, 138272 (2021).
[40]A. J. Samin and J. C. Petrosky, "An analysis of point defects in ZnTe using density functional theory calculations," J. Alloys Compd. **921**, 166017 (2022).
[41]M.. Shkir, M. T. Khan, I. M. Ashraf, A. Almohammedi, E. Dieguez, and S. AlFaify, "High-performance visible light photodetectors based on inorganic CZT and InCZT single crystals," Sci. Rep. **9**(1), 12436 (2019).
[42]C. Zhang, R. Sa, and D. Liu, "The influence of minor Mg doping on the physical properties of CdTe: A DFT study," Chem. Phys. **562**, 111674 (2022).
[43]C. Soykan and S. Özdemir Kart, "Structural, mechanical, and electronic properties of ZnTe polymorphs under pressure," J. Alloys Compd. **529**, 148–157 (2012).

02 November 2026 18:33:59

© Author(s) 2026